Detection, Analysis and Matching of Hair

Yaser Yacoob and Larry Davis
Computer Vision Laboratory
University of Maryland
College Park, MD 20742
yaser/lsd@umiacs.umd.edu

Abstract

We develop computational models for measuring hair appearance for comparing different people. The models and methods developed have applications to person recognition and face image indexing. An automatic hair detection algorithm is described and results reported. A multidimensional representation of hair appearance is presented and computational algorithms are described. Results on a dataset of 524 subjects are reported. Identification of people using hair attributes is compared to Eigenface-based recognition along with a joint, Eigenface-hair based identification.

1 Background

Hair is an important feature of human appearance but its detection, representation, analysis and use have not been studied in the computer vision community. Hair analysis has at least two potential applications areas: human identification and image indexing of faces. It has been suggested [13] that humans employ hair as a cue for face recognition. Specifically, it was shown that hair is a prominent cue and that changes in hair-style or facial hair can mislead the observer in the recognition of faces. Also, [2] contends, based on a survey of cue saliency, that hair is the most important single feature for recognizing familiar faces, suggesting that it should be advantageous to use in recognition. Since hair appearance and attributes can so easily be changed, they have been widely regarded as unstable features for face recognition. The fact is, however, that while humans *can* drastically manipulate their hair to significantly alter their appearance, they typically *do not* do so. Moreover, there are variety of situations (e.g., face partial occlusion, side and back views) where face recognition is not viable, yet hair may provide a useful cue for identification. Identity verification can also benefit from evaluation of hair properties.

We are not aware of any prior work on hair detection, representation and use in the computer vision or image processing communities. However, hair has been an important research topic in computer graphics and animation [5, 8].

An extensive discussion of hair properties and associated attributes can be found in [1]. Hair can be represented along the following dimensions: *length*, *volume*, *surface area*, *dominant Color*, *coloring* (i.e., color variations), *forehead/outer hairline*, *density*, *baldness*, *symmetry*, *split location*, *reflectance/shine*, *structural alteration*: (e.g., banded, layered or braided hair), *layering arrangement*, *texture*, *sideburns*, *facial hair cover*, In the rest of the paper we address several of these dimensions. Structural alterations, layering, density and facial hair are not addressed due to the difficult challenge of 3D recovery of shape properties or the difficulty of observing them in typical image resolutions.

2 Approach

A dataset of 524 color images of subjects (1600x1200 and 768x576 pixels) taken in several locations (hair salons, on campus, social events) and over a period of a few months was collected (multi-ethnic and balanced numbers of males and females). Out of these, 126 faces were taken from the Aleix Martinez and Robert Benavente database [9]. This dataset is used to evaluate the similarity between the hair of subjects based on *individual* attributes of their hair. A second dataset consisting of over 3100 images (126 subjects) taken from Aleix Martinez and Robert Benavente database [9] is employed to assess the performance of person-identification from single hair attributes, aggregate hair, eigenface-based, and combined eigenface and hair based information.

2.1 Hair Detection

Hair is a highly variable feature of human appearance; it perhaps is the most variant aspect of human appearance. Its automatic detection is challenging;

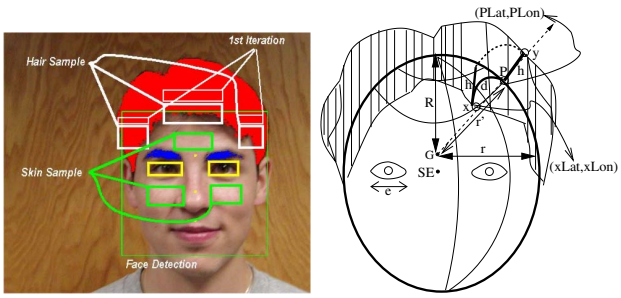

Figure 1: Region selection for hair detection (left) and Approximate model of the head (right).

we describe an algorithm for automatic detection of hair. We assume that faces are in frontal view. The detection algorithm consists of the following steps (the first two are available in the public domain and are not described in detail here):

- **Face detection**. Face detection has been reported by many researchers (e.g., [6, 12]). We employ the algorithm based on a cascade of boosted classifiers (part of Intel's OpenCV) to detect face regions in the image [6].
- **Eye detection**. We also use the cascade of boosted classifiers to train eye detectors to locate the eyes within a face region. Face and eye detection allow us to normalize face sizes so hair representations can be compared.
- **Skin color modelling**. The subject-specific skin color is modelled based on automatic selection of three regions, two are below the eyes and one at the forehead (see Figure 1 -left). The color model follows [4] and is discussed in Section 2.2. This skin modeling approach takes into account the possibility that some non-skin pixels may be present in the rectangles.
- **Head hair color modeling**. Hair is assumed to be present at one or more of three principle locations adjacent to facial skin, namely, right, middle and left sides of the upper face (thick white rectangles in Figure 1-left). The initial areas are automatically set based on the location of the detected face and eyes. The skin color model is used to identify non-skin pixels in these regions, and these pixels form the seed to separately model the hair color in each region. If the distance between the three colors (i.e., the distance between the means of the RGB values of the colors) is small, then the overall color is recalculated using the pixels of the three regions, otherwise the color is computed at the forehead rectangle and is assumed to be the seed color. The seed color is iteratively refined by computing the model of the color of the rectangles above each of the current rectangles, and examining if this color is close to the seed color. If it is close, the current model is recalculated. The process ends when the color of a rectangle is not close to the seed color. Standard image processing techniques are used to fill in holes in the hair region and create a connected component.

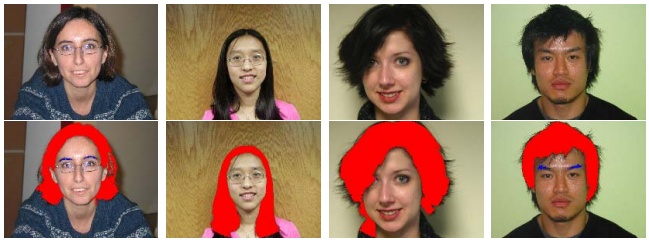

Figure 2: Successful automatic hair detection

Figure 3: Unsuccessful hair detection

Figure 1(left) shows an example of automatic hair detection. The face and eyes are detected and shown. The skin-color sampling areas are shown as three green rectangles and the initial three sampling areas for the hair are shown as thick white rectangles. The thinner rectangles show the first iteration of the (upward) neighboring rectangle assessment. The detected hair and brows are shown in red and blue (respectively). Figure 2 shows successful head hair detection of five subjects. Figure 3 shows unsuccessful head hair detection.

This automatic hair detection procedure achieved a 71% success on head hair detection on the 526 face dataset (as judged by visual inspection). However, it achieved 93.6% on the 126-face dataset [9]. This is probably due to the fact that the latter dataset was taken under controlled conditions whereas our dataset was collected by hair-stylists in public spaces. Several issues affect the performance of our algorithm: overlap of actual hair color with background regions (Figure 3, left), determining that a subject has no or little hair (Figure 3,

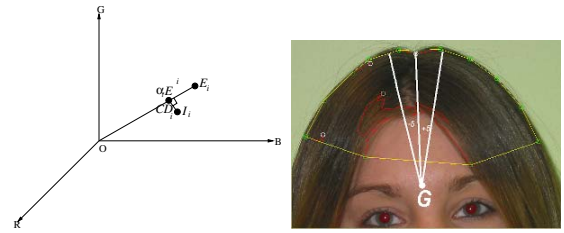

Figure 4: Illustration of brightness and chromaticity color model (left) and hair shine (right).

second from the left), and detection of the hair of subjects with multiple hair colors cannot be accomplished with our algorithm because of the color coherence assumption around the facial skin (Figure 3, rightmost two pictures). To focus on the objective of representing hair, in the experiments below we manually performed hair detection for the 29% cases where the algorithm did not provide acceptable results.

2.2 Hair Color

The computer graphics community has developed models that seek to render hair realistically [5, 8]. The most widely used model was proposed by Kajiya and Kay [5] who employed a Lambertian surface model to represent the diffuse component (reflecting brightness) of a single hair represented as a cylinder. The specular component of hair employed a Phong reflection model that was modified to a cylindrical surface. We employ a similar model that assume that hair is Lambertian so the measured color results from brightness and surface spectral reflectance. A model that separates these two components can facilitate color constancy detection by focusing on the surface spectral reflectance component. Specifically, the color model (see [4]) accounts for highlights and shadows that often affect the brightness of the color of the hair. Figure 4(left) illustrates the color model proposed in [4]. In the figure $E_i = (E_r(i), E_g(i), E_b(i))$ represents the expected (modeled) color RGB values at pixel i and $I_i = (I_r(i), I_g(i), I_b(i))$ is the actual RGB color at pixel i. The line OE_i is called the expected chromaticity line. The distortion between I_i and E_i can be attributed to brightness and chromaticity by observing that brightness similarity is equivalent to bringing the point I_i to the line OE_i and can be posed as minimization of the error

$$f(\alpha_i) = (I_i - \alpha_i E_i)^2 \quad (1)$$

where α_i represents the current brightness with respect to the brightness of the model (being greater than 1 if it is more bright, i,e., highlighted, and less than 1 if it is less bright, i.e., shadowed). Color distortion, CD_i, is defined as:

$$CD_i = ||I_i - \alpha_i E_i|| \quad (2)$$

Computing a hair color model involves using sample pixels from the subject's hair to estimate a 4-tuple $< E_s, d_s, a_s, b_s >$ where E_s is the mean (R, G, B) value for the color, d_s is the standard deviation of the color training set, a_s is the variation of the brightness distortion among the points in the training set and b_s is the variation in the chromaticity among these points. This model is employed to classify colors while accounting for shadows and highlights as particular brightness values with respect to the model. A pixel i is classified as matching the color model based on the observed distortion value α_i that is computed with respect to the color model. A threshold value is used to accept the brightness and chromaticity deviation from the color model. Specifically, a pixel is classified by first computing the distortion α_i

$$\alpha_i = \frac{(I_r(i)\mu_r/\sigma_r)^2 + (I_g(i)\mu_g/\sigma_g)^2 + (I_b(i)\mu_b/\sigma_b)^2}{(\mu_r/\sigma_r)^2 + (\mu_g/\sigma_g)^2 + (\mu_b/\sigma_b)^2} \quad (3)$$

and CD_i

$$CD_i = \sqrt{(\frac{I_r(i) - \alpha_i\mu_r)}{\sigma_r})^2 + (\frac{(I_g(i) - \alpha_i\mu_g)}{\sigma_g})^2 + (\frac{(I_b(i) - \alpha_i\mu_b)}{\sigma_b})^2} \quad (4)$$

where (μ_r, μ_g, μ_b) is the mean of the color in the training set and $(\sigma_r, \sigma_g, \sigma_b)$ is the standard deviation of this set. A point is classified as matching the color model if the computed CD_i is smaller than a preset threshold and α_i falls in value between two thresholds that are determined automatically based on the desirable detection rate of the color in the training region.

The distance between the means of the *dominant* hair color of two subjects measures the similarity of their hair colors. Figure 5 (left) shows the closest five matches of hair color to the left most person in each row. The normalized distance between subjects and the left most subject is shown as a red bar in which its length decreases as the distance between subjects increases. These are few samples from the cross-subject similarity of the whole dataset of 524 subjects (all following results in this section use this dataset).

2.3 Hair-Split Location

A hair split location commonly appears as either a darker shade of the hair color (along the split location) or as revealed skin within the hair region (Figure 4, right). Also, a split is accompanied by a concavity point at the outer hairline and/or the

Figure 5: Dominant Color results. The closest five matches to the subject at the left of each row are shown. The longer the red bar the closest the distance is between each subject and the leftmost subject.

forehead. The person-specific skin and hair color models are used to detect the presence of a hair split and its location. For each concavity point on the outer and forehead hairline at the upper part of the head, the mean of the color adjacent to the line connecting this point to the glabella (G in Figure 4) is computed and compared to the shadowed skin and hair color models. Also, the mean of the colors adjacent to the lines ± 5 degrees off this line are computed (4, right). Figure 4 (right) shows the lines in the case of successful split detection. If the hair color is dark (e.g. black) and no skin is visible, a split may exist if there are two concavity points, one at the outer hairline, and another at the forehead hairline that fall approximately on a straight line with the glabella.

A split is defined by the angle it creates with respect to the horizontal axis. Splits are compared based on the difference between their respective angles. Figure 6 (top) shows the closest five matches of split-location to the left most subject in each row.

2.4 Hair Volume

We employ an approximate model for the head utilizing anthropometric information [3] (Figure 1(right)). The location of the point SE (center point between the two eyes, computed at the detection stage) is used to determine the location of the glabella G (the horizontal coordinates for G and SE are equal, and the vertical coordinate of G is 1.8 times the height of the eye upward from SE). The top half of the skull is assumed to be a spheroid with the minor axis r as the distance be-

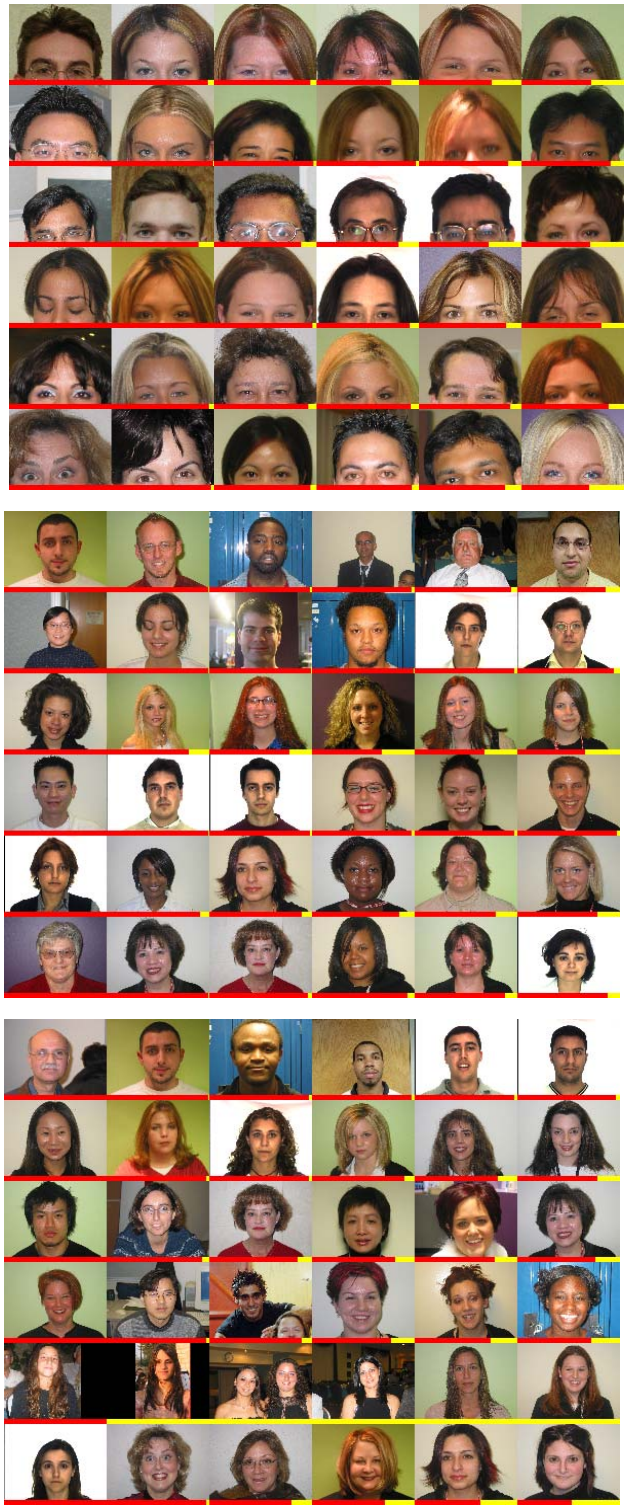

Figure 6: Hair split, volume and length (top to bottom, respectively) closest five matches to the left most subject.

tween the glabella, G, (approximately the meeting point of eyebrows) and the top of the ear. The major axis distance, R, (which is the distance between the glabella and the top of the skull) is calculated using anthropometric statistics indicating that the average ratio between the major and minor axes is approximately 1.35 [3]. The value r of the minor axis is computed from the average eye width in the image, e to be $r = (e * (151.1/31.3))/2$, where 151.1mm is the average head width at the glabella and 31.3mm is the average eye fissure.

Each image pixel within the rendered spheroid (parameterized by r and R) can be associated with a latitude and longitude in the same way the spheroid Earth is described. The 3D distance, d, between two points is computed given the latitude and longitude of these points.

The area is divided into 624-sectors covering 360 degrees. As we move along each sector the radius, r', is $r' = \sqrt{(r^2 cos^2\theta + (1.35r)^2 sin^2\theta)}$. Within each sector, we calculate the average hair length (i.e., $h = y - r'$ see Figure 1 Right). The inner hairline boundary (which is at a perpendicular distance x from G) indicates, approximately, which portion of the *visible* part of the spheroid is covered by hair.

The space occupied by the hair of a sector is computed as the 3D distance, d, on the spheroid between x and P (where P is the hypothesized projected edge of the spheroid) multiplied by the hair height h (assuming hair length is constant along the sector). The hair volume is a summation of the space occupied by the hair of all sectors. Note that if $x > P$, the volume of the sector is equal to the distance $y - x$, and $d = 1$; this also accounts for the volume calculation of the hair found below the level of the ears. Figure 6 (middle) shows the closest five volume matches to the leftmost subject in each row.

2.5 Hair Length

Hair length is computed as the larger of the distance between the spheroid boundary, P, and the outer-hairline boundary y, and the inner-hairline boundary x and P (see Figure 1 (right)). Hair below the ears is assumed to grow at the horizontal line passing through the glabella so in effect the growth is from the top of the ear level, which is approximately the midpoint of the skull. The length is the vertical distance between the hair boundary point and the vertical coordinate of the ear. The hair length is computed across all the points and the largest value is taken as the hair length

$$h = \max_{\alpha}(y - P, x - P) \quad (5)$$

where α is the sweep angle. Figure 6 (bottom) shows the closest five matches to hair length of the left most subject.

2.6 Surface Area Covered by Hair

The surface area covered by hair is computed for the top of the head (above eye-level) using the spheroid head model. This area is divided into sectors similar to Section 2.4. The distance d (between the points x and P) is computed using the latitude and longitude of the two points. The surface area is the summation of the distances, d, in all sections above the ear level. Figure 7 (top) shows the closest five matches to surface area of the left most subject. Note that baldness is readily reflected in diminishing surface area (second row).

2.7 Hair Symmetry

The head is divided into left and right sides and the ratio of the volumes of hair (V_{right}/V_{left}) reflects the degree of symmetry. Figure 7 shows the closest five matches hair symmetry to the left most subject from among the 50 faces that are closest in terms of the total hair volume (so that symmetry and total volume are linked).

2.8 Inner and Outer Hairlines

The similarity between the hairlines of subjects is calculated as a function of the outer and inner hairlines. The inner and outer hairlines of subjects are reparameterized using a radial scan with respect to the glabella and normalized by the face size. Then, the inner and outer hairlines are each normalized to a fixed-size, $624 * 2$ units spanning 360 degrees. Principal Component Analysis computes the subspace of the concatenated (inner and outer) hairline vectors (after subtracting the mean of the exemplars). In our experiments we found that 15 principal vectors are sufficient to capture more than 95% of the variability of the hairline. The distance between two subjects is computed as the Euclidean distance between their respective coefficients in the PCA subspace. Figure 7 (bottom) shows the closest five matches of hairline to the leftmost subject.

2.9 Hair Texture

We adopt the method proposed by Manjunath and Ma [7] for computing hair texture features. The method employs Gabor wavelets to compute a feature vector that can be used for matching different

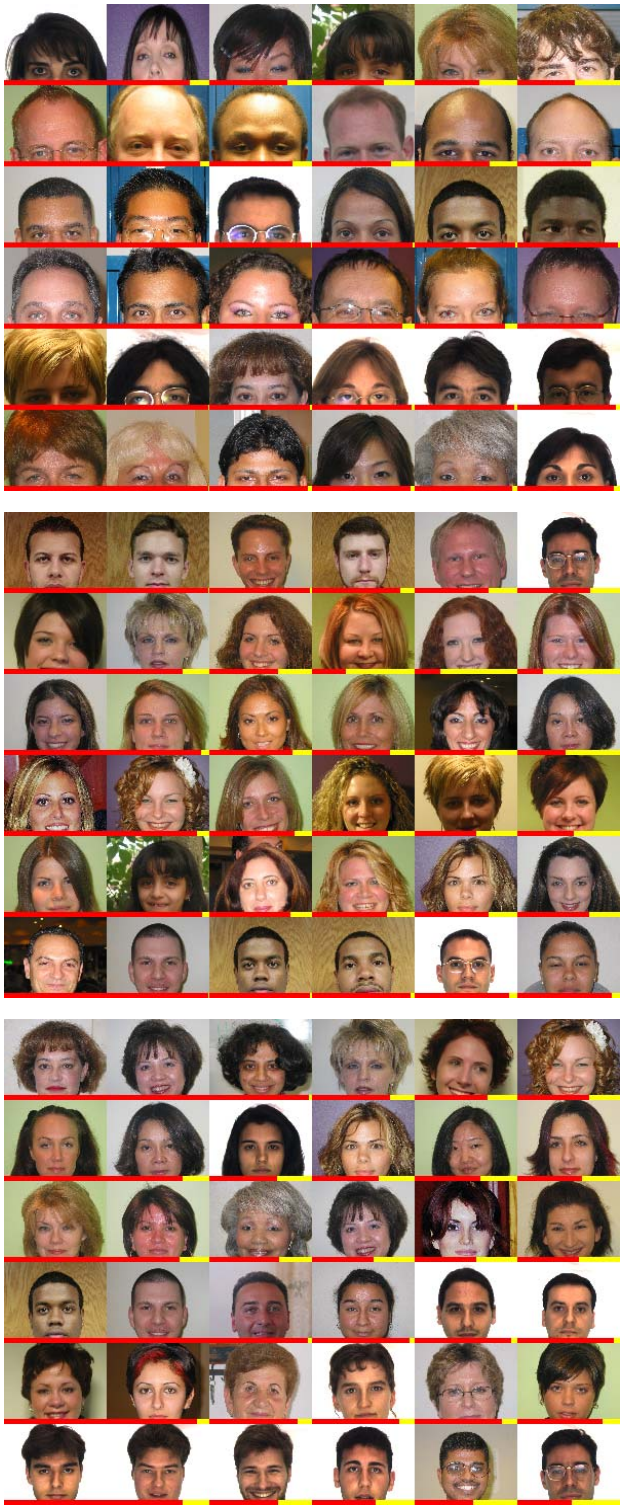

Figure 7: Surface area, symmetry and hairlines (top to bottom, respectively) closest five matches to the left most subject.

Figure 8: The closest five matches of hair texture to the left most subject.

images. Given a hair region, we extract all 64x64 non-overlapping templates. The difference in texture between two subjects ${S_1}^P$ and ${S_2}^Q$ (P and Q are the number of templates), is defined as

$$D_{12}^{PQ} = [\sum_{i=1}^{P} min_{j=1}^{Q} d(i,j)]/P \tag{6}$$

where $d(i,j)$ is the distance between template i and j as defined in [7]. This essentially sums the minimum distance between each template of ${S_1}^P$ and the closest template of ${S_2}^Q$. It should be noted that ${D_{12}}^{PQ}$ is not equal to ${D_{21}}^{QP}$ and therefore two subjects' hair have similar texture only if ${D_{12}}^{PQ}$ and ${D_{21}}^{QP}$ are both small and similar in value. Define

$${M_{12}}^{PQ} = [\sum_{i=1}^{P} \frac{\sum_{j=1}^{Q} d(i,j)}{Q}]/P \tag{7}$$

which reflects the average distance between all templates of ${S_1}^P$ and all the templates of ${S_2}^Q$. This distance satisfies ${M_{12}}^{PQ} = {M_{21}}^{QP}$. The total normalized distance between ${S_1}^P$ and ${S_2}^Q$

$${T_{12}}^{PQ} = {M_{12}}^{PQ} / \min_q {M_{1q}}^{Pq} + {D_{12}}^{PQ} / \min_q {D_{Pq}}^{Pq} \tag{8}$$

where q is calculated over all the subjects in the dataset. Figure 8 shows the closest five matches of hair texture to the left most subject.

3 Human Identification

We present an experiment that measures the effectiveness of the hair representation and attributes for human identification. We compare the results to eigen-face recognition [14]. We use the Aleix Martinez and Robert Benavente (AR) dataset [9], which includes about 26 images of 126 subjects (some subjects have fewer than 26 images). A total of 3153

images are employed. The images were taken of the subjects at two sessions (2 weeks apart), 13 images each session; face expression, lighting, eye-glasses and neck/head cover were used to disguise or alter the appearance of the individual. Note that the sunglesses and scarf-worn images are extremely challenging and to our knowledge have been tackled only in [10] by dividing the face region into a fixed number of regions which are analyzed in isolation before results are aggregated.

We employed our hair detection algorithm and determined that the detection of hair in 2709 (%86) images was acceptable. We divided the 2709 images into gallery and probe images. The gallery consists of a single image of each person taken in the neutral position (face, light and no wearable artifacts). The probe images consist of all the rest. Thus, on average 25 probe images of each subject are matched against the 126-subjects gallery.

R	Hairline	Texture	Length	Surface
1	10.2(14.9)%	19.6(21.0)%	3.4(3.9)%	1.9(2.5)%
2	14.2(20.0)%	26.5(28.5)%	5.9(6.8)%	3.3(4.1)%
3	18.4(25.1)%	30.7(32.8)%	8.2(9.4)%	4.6(5.8)%
4	21.4(28.6)%	34.8(36.1)%	10.6(11.9)%	6.0(7.4)%
5	24.0(31.7)%	37.6(38.5)%	13.4(15.2)%	7.4(9.2)%
6	26.1(33.6)%	40.0(40.9)%	15.6(17.5)%	8.5(10.5)%
R	Symmetry	Volume	Color	Split
1	1.8(2.2)%	2.9(3.6)%	8.5(11.5)%	3.6(2.9) %
2	3.0(3.2)%	5.7(6.4)%	12.0(15.5)%	7.5(6.2)%
3	4.6(5.1)%	8.2(9.1)%	14.7(18.3)%	12.2(10.5)%
4	6.3(7.1)%	10.5(11.8)%	17.2(20.9)%	14.8(13.5)%
5	7.5(8.4)%	13.0(15.2)%	19.4(23.7)%	17.3(14.8)%
6	8.8(9.6)%	15.2(17.5)%	21.1(25.1)%	20.0(16.7)%

Table 1: Correct identification using hairline, texture, length, surface area, symmetry, volume and color, split location as a function of rank-R (in parentheses the results are for the dataset excluding the sun-glasses and scarve-warn images).

We pose the following classification task: for each probe and each hair attribute rank the closest subject from the gallery. Table 1 displays the success in matching probe and gallery (percentage wise) as a function of how well the correct identification was ranked. We consider only the top six ranked subjects for each probe query. For example, the left most column shows that about 26.1% of the probes were ranked within the 6 top matches when the hairline attribute was used, while 10.2% were identified correctly as the best ranked. The texture attribute scored the best, with 19.6% of the subjects matched successfully despite the significant lighting variations in these images. The attributes that scored the least were volume, surface area, symmetry, split and length. The length, volume, surface and symmetry are closer in value for many subjects (specifically, males with short hair). Hair splits were observable or detectable for only a subset of the dataset and therefore they were not helpful for probes that lacked them. Since in many of the images the hair are partially covered we excluded all images with sun-glasses or head scarves to determine how the identification performance changes. Table 1 (numbers in parentheses) show slightly improved identification performance for all hair attributes.

We compare the human identification potential of hair attributes to the well-known Eigenface, Principal Component Analysis (PCA), approach [14]. The images were cropped, registered and warped automatically so that the same inaccuracies affecting the hair attribute identification affect the PCA-based approach. We also obtained manually registered images of the same AR dataset from [9] to evaluate the performance of ideal registration of faces. Table 1 (right column) shows the performance of PCA-based recognition on the whole dataset for the manually registered images. The performance is worse than the typical PCA performance since this dataset is considerably more diverse in imaging and facial parameters. No similar results are reported in [10] but the occlusion results reported in [10] appear close in value. The second column from the right shows the identification rates for our automatically registered face images. We observed inaccurate registration of images of subjects wearing sun-glasses, scarves and highly deformed faces during face expressions. Note that several hair attributes showed comparable (for manually registered PCA) or better (for automatically registered PCA) performance with respect to the Eigenface results on the full database.

Since hair attributes and PCA are independent, we use the ranking of subjects based on their hair attributes and PCA to compute a single ranking. To aggregate the ranking of hair attributes, we choose the 3 best ranked attributes for each probe. For example, a probe P_i matched to the gallery G_j leads to the hair attributes rank values $r_1, r_2, ..., r_N$ with respect to the complete gallery G (where N is the number of hair attributes). We choose the best three ranks out of these N and their average $v(i,j)$ is considered the degree of hair-match between P_i and G_j hair. The average $v(i,j)$ is averaged with the PCA-based rank of the probe to provide an identification rank. This average is a vari-

R	Auto. Reg. PCA-Hair	Manu. Reg. PCA-Hair	Hair	Auto. Reg. PCA	Manu. Reg. PCA
1	19.3(29.7)%	29.0(40.0)%	17.9(23.2)%	12.1(20.7)%	24.1(35.8)%
2	25.3(36.7)%	38.0(48.7)%	25.4(31.6)%	16.1(26.6)%	31.3(43.0)%
3	29.5(41.4)%	43.8(54.6)%	31.2(37.7)%	18.9(31.0)%	36.1(47.9)%
4	32.3(44.4)%	48.2(58.7)%	34.9(41.5)%	21.7(34.7)%	39.3(50.6)%
5	34.7(47.0)%	51.5(62.0)%	38.0(44.7)%	23.8(36.8)%	43.1(53.9)%
6	36.8(49.1)%	55.0(64.7)%	41.2(47.6)%	26.1(39.6)%	45.4(55.7)%

Table 2: Correct identification using (from left to right): joint hair attributes and PCA of automatically registered images, joint hair attributes and PCA of manually registered images, hair attributes alone, PCA of automatically registered images, and PCA of manually registered images.

ation on the Highest Rank Classifier [11] that is an effective method to combine classifier output. Table 2 (parentheses) shows the recognition results for correct identification ranks of $1, ..., 6$ for the whole dataset using the combined hair-PCA information (where automatic registration of images for PCA is used). The second column (from the left) shows the results for hair and manually registered eigenface images. The results show about 20-30% improvement over the PCA based ranking given in Table 2 and improvement with respect to the hair-based recognition only in the case of manually registered images (third column from the right). Table 2 (left column) shows the results for the dataset that excludes the images of subjects wearing sun-glasses and scarves (clearly problematic for PCA) and it shows clear improvement. In this case, the combination of hair and PCA surpassed the other identification methods, achieving 49.1% and 64.7% correct identification for automatic and manually registered images.

4 Summary

A set of attributes of the head hair that can be estimated from a single image was presented. Algorithms and associated metrics that enable detection, representation and comparison of the hair of different subjects were described. A large dataset consisting of 524 subjects was used to illustrate the qualitative performance of the algorithms. We also used a set of over 3100 images taken from the AR dataset [9] to quantitatively assess the consistency, viability and performance of the algorithms under significant variations of hair appearance in the task of human identification. An approach for combining PCA and hair classification has been proposed. A rank-based analysis of hair attributes and PCA has shown that identification can be improved even under challenging imaging conditions.

References

[1] A. Charles and R. DeAnfrasio. *The History of Hair*. Bonanza Books, New York, 1970.

[2] G.M. Davies, H.D. Ellis and J.W. Shepherd, Editors. Perceiving and Remembering Faces. Academic Press Series in Cognition and Perception. Academic Press, London, 1981.

[3] L. Farkas. *Anthropometry of the head and face.* Second Edition.

[4] T. Horprasert, D. Harwood, and L.S. Davis, A Statistical Approach for Real-time Robust Background Subtraction and Shadow Detection, ICCV FRAME-RATE Workshop, 1999.

[5] J.T. Kajiya, and T.L. Kay, Rendering fur with three dimensional textures. Computer Graphics, 23(3), 1989, 271-280.

[6] R. Lienhart, L. Liang, and A. Kuranov. A Detector Tree of Boosted Classifiers for Real-time Object Detection and Tracking. IEEE ICME2003, July 2003.

[7] B.S. Manjunath and W.Y. Ma. Texture Features for Browsing and Retrieval of Image Data. *PAMI*, (18)8, 1996, 837-842.

[8] S.R. Marschner, H.W. Jensen, M. Cammarano, S. Worley, and P. Hanrahan, Light Scattering from Human Hair Fibers. SIGGRAPH 2003, 780-791.

[9] A. Martinez and R. Benavente, "The AR-face Database", CVC Technical Repoer #24, June 1998, Purdue University.

[10] A.M. Martinez, Recognizing Imprecisely Localized, Partially Occluded and Expression Variant Faces from a Single Sample per Class, *PAMI*, 24(6), 2002, 748-763.

[11] O. Melnik, Y. Vardi, Z. Cun-Hui, Mixed Group Ranks: Preference and Confidence in Classifier Combination *PAMI*, 26(8), 2004, 973-981.

[12] H.A. Rowley, S. Baluja and T. Kanade. Neural Network-Based Face Detection. *PAMI*, 21(1), 1998, 23-38.

[13] Sinha, P. and Poggio, T. United we stand: The role of head-structure in face recognition, Perception, 31/1, 2002, 133.

[14] M. Turk, and A. Pentland, Eigenfaces for recognition. Journal of Cognitive Neuroscience, 3, 1991, 71-86.